# El Niño Modoki I and II Classifying by Different Impacts on Rainfall in Southern China and Typhoon Tracks

Chunzai Wang [1]

Xin Wang [2 & 1]

[1] NOAA Atlantic Oceanographic and Meteorological Laboratory

Miami, Florida

[2] Cooperative Institute for Marine and Atmospheric Studies

University of Miami

Miami, Florida

*Journal of Climate*

August 2012

Corresponding author address: Dr. Xin Wang, Physical Oceanography Division, NOAA/Atlantic Oceanographic and Meteorological Laboratory, 4301 Rickenbacker Causeway, Miami, FL 33149.
E-mail: Xin.Wang.AOML@noaa.gov.

## Abstract

Based on the opposite influence on rainfall in southern China during boreal fall, this paper classifies El Niño Modoki into two groups: El Niño Modoki I and II which show different origins and patterns of SST anomalies. The warm SST anomalies originate in the equatorial central Pacific and subtropical northeastern Pacific for El Niño Modoki I and II, respectively. Thus, El Niño Modoki I shows a symmetric SST anomaly distribution about the equator with the maximum warming in the equatorial central Pacific, whereas El Niño Modoki II displays an asymmetric distribution with the warm SST anomalies extending from the northeastern Pacific to equatorial central Pacific. Additionally, the warm SST anomalies in the equatorial central Pacific extend further westward for El Niño Modoki II than El Niño Modoki I. Similar to canonical El Niño, El Niño Modoki I is associated with an anomalous anticyclone in the Philippine Sea which induces southwesterly wind anomalies along the south coast of China and carries the moisture for increasing rainfall in southern China. For El Niño Modoki II, an anomalous cyclone resides east of the Philippines, associated with northerly wind anomalies and a decrease in rainfall in southern China. Canonical El Niño and El Niño Modoki I are associated with a westward extension of the western North Pacific subtropical high (WNPSH), whereas El Niño Modoki II shifts the WNPSH eastward. Differing from canonical El Niño and El Niño Modoki I, El Niño Modoki II corresponds to northwesterly anomalies of the typhoon steering flow which are unfavorable for typhoons to make landfall in China.

## 1. Introduction

The El Niño-Southern Oscillation (ENSO) phenomenon greatly affects climate variations in China (e.g., Chang et al. 2000; Wang et al. 2000; Wang and Zhang 2002; Li et al. 2006; Zhou and Chan 2007; Zhou et al. 2007a). ENSO is an important predictor for regional seasonal climate over East Asia. The relationships between ENSO and the East Asian climate are very complex and have recently been suggested to change on inter-decadal timescales (Wu and Wang 2002; Zhou et al. 2007b; Xie et al. 2010; Wang et al. 2012). It is well known that the interannual climate variation over East Asia is significantly related to the ENSO cycle (e.g., Huang and Wu 1989; Wang et al. 2000). Huang and Wu (1989) suggested that summer rainfall anomalies in China are different during the developing and decaying phases of ENSO. Wu et al. (2003) further studied the El Niño-related rainfall anomaly pattern over East Asia during the various phases of El Niño. The ENSO-related positive rainfall anomalies migrate from southern China in the developing phase of ENSO, eastward in the mature phase of ENSO, and northeastward to eastern central China and southern Japan in boreal spring during the decaying phase of ENSO, in association with the changes of low-level atmospheric circulation in the western North Pacific. In addition, the negative rainfall relationships are seen in northern China in summer and fall of the ENSO onset year, which is associated with the anomalous barotropic cyclone displacing southwestward along the East Asian coast.

Recently, a different type of El Niño called El Niño Modoki (Ashok et al. 2007) has been emphasized because its maximum sea surface temperature (SST) anomalies are located in the tropical central Pacific instead of being in the tropical eastern Pacific as for canonical or conventional El Niño. Modoki in Japanese means “a similar but different thing”. El Niño Modoki is also named as “Date Line El Niño” (Larkin and Harrison 2005), “Central Pacific El

Niño" (Yu and Kao 2007) or "Warm Pool El Niño" (Kug et al. 2009). Its impacts on the tropical and mid-latitude climate are distinct from these of canonical El Niño because the intensity and locations of their associated SST-induced heating are different (e.g. Larkin and Harrison 2005; Ashok et al. 2007; Weng et al. 2007 and 2009; Cai and Cowan 2009; Kim et al. 2011).

The influences of El Niño Modoki during different El Niño phases over East Asia have been documented and compared with these of canonical El Niño (Weng et al. 2007 and 2009; Ashok et al. 2007; Feng and Li 2011; Feng et al. 2011; Zhang et al. 2011). Weng et al. (2007, 2009) and Ashok et al. (2007) analyzed the impacts of El Niño Modoki in boreal summer and winter of the El Niño developing year. The composite and partial correlation analyses illustrated that El Niño Modoki greatly influences the rainfall anomalies over the maritime regions, India, southern Japan, and eastern Australia in summer, while its influences on rainfall in China in summer are weak (Ashok et al. 2007). During winter of the El Niño developing year, different atmospheric anomalous circulation patterns in the western North Pacific result in different rainfall impacts on southern East Asia between canonical El Niño and El Niño Modoki (Ashok et al. 2007; Weng et al. 2009). During fall of the El Niño developing year, Zhang et al. (2011) showed that canonical El Niño is associated with increased rainfall over southern China, but El Niño Modoki corresponds to insignificant rainfall changes in southern China (see their Fig. 3). During spring of the El Niño decaying year (the subsequent spring of El Niño mature year), Feng and Li (2011) and Feng et al. (2011) pointed out opposite rainfall changes between canonical El Niño and El Niño Modoki.

Canonical El Niño and El Niño Modoki are not independent. Using the monthly Nino3 and El Niño Modoki indices from 1910-2010 (see Section 2 for the definitions of these indices), we found that the correlation is 0.23 (above the 95% significant level). We calculate the partial

correlation maps of rainfall in China with the canonical El Niño and El Niño Modoki indices for four seasons (Fig. 1). Consistent with previous studies, canonical El Niño is associated with an increase of rainfall in southern China especially during fall and winter. However, El Niño Modoki does not show a significantly positive rainfall correlation in southern China. This suggests that the link between El Niño Modoki and the southern China rainfall may be complex and the correlation may not represent the true relationship between El Niño Modoki and the southern China rainfall. The present paper mainly focuses on the relationships of El Niño events with the southern China rainfall during fall. We find that because some El Niño Modoki events show positive rainfall anomalies in southern China and others display negative rainfall anomalies, the correlation in Fig. 1 shows an insignificant relation. Based on the opposite impacts on rainfall in southern China, El Niño Modoki events can be divided into two groups: El Niño Modoki I and II, which also show different origins and patterns of SST anomalies, and different atmospheric circulations in the western North Pacific. The present paper also investigates physical mechanisms of rainfall relationships and examines the influences of various El Niño events on the typhoon tracks in the western North Pacific.

The paper is organized as follows. Section 2 introduces the data sets and indices used in the study. Section 3 analyzes the relationships between the anomalous precipitation over southern China and El Niño events and identifies two groups of El Niño Modoki based on the rainfall pattern in southern China. Section 4 shows different SST anomaly spatial patterns and evolution of various El Niño events. Section 5 examines El Niño-related atmospheric circulations in the western North Pacific and East Asia, and explains why various El Niño events have different rainfall influences in southern China. Section 6 uses a simple atmospheric model to show atmospheric response to various El Niño events. Section 7 investigates the influences of

various El Niño events on the typhoon tracks in the western North Pacific. Finally, section 8 provides a summary and discussion.

## 2. Data sets and numerical model

### *a. Data sets*

Several observational and reanalysis data sets are used in this study. The atmospheric reanalysis data sets include the National Centers for Environmental Prediction-National Center for Atmospheric Research (NCEP-NCAR) reanalysis (Kalnay et al. 1996) and the newly developed NOAA Earth System Research Laboratory (ESRL) 20$^{th}$ Century Reanalysis (20CR) (Compo et al. 2011). The NCEP-NCAR reanalysis has a spatial resolution of 2.5°×2.5° and the 20CR reanalysis has a resolution of 2.0°×2.0°. We analyze both the NCEP-NCAR reanalysis and the 20CR reanalysis. For the overlapping period from 1950 to 2010, the two reanalysis data sets show similar results. Because we would like to use a longer-period data set (with a large sample size, especially for El Niño Modoki events), we present the results from the 20CR reanalysis for the period of 1910 to 2010 in this paper.

The rainfall data set is from the Global Precipitation Climatology Centre (GPCC). The monthly rainfall data are gridded from the complete GPCC station database with more than 70,000 different raingauge stations worldwide (Rudolf et al. 1994). The gridded land precipitation is available in spatial resolutions of 0.5°×0.5° and 1.0°×1.0°. Here we use the precipitation with the resolution of 1.0°×1.0° from 1910 to 2010. The rainfall data are available from http://www.esrl.noaa.gov/psd/data/gridded/data.gpcc.html. Monthly SST from the Hadley Centre Sea Ice and SST data set (HadISST) on a 1.0°×1.0° resolution from 1910 to 2010 is used (Rayner et al. 2003).

Following the annual reports of "State of The Climate" in the Bulletin of the American Meteorological Society, all anomalies are calculated as departures from the 1971-2000 climatology. The Nino3 index obtained from the Japan Meteorological Agency, which is the 5-month running mean SST anomalies in the region of 150°W-90°W, 5°S-5°N, is used to define canonical El Niño. El Niño Modoki is identified by the El Niño Modoki Index (EMI) defined by Ashok et al. (2007) as:

$$EMI = [SSTA]_C - 0.5\times[SSTA]_E - 0.5\times[SSTA]_W,$$

where the brackets with a subscript represent the area-averaged SST anomalies (SSTA) over the central Pacific region C (165°E-140°W, 10°S-10°N), the eastern Pacific region E (110°W-70°W, 15°S-5°N) and the western Pacific region W (125°E-145°E, 10°S-20°N), respectively.

The tropical cyclone (TC) data set from the website of the International Best Track Archive for Climate Stewardship (IBTrACS) Project (http://www.ncdc.noaa.gov/oa/ibtracs/) is used in this study. Because of TC data availability and reliability in the western North Pacific (e.g., Song et al. 2010; Ren et al. 2011), the TC data set used in this study is from 1950 to 2010.

*b. Numerical model*

To examine the responses to tropical heating anomalies associated with various El Niño events, we also use a simple atmospheric model developed by Lee et al. (2009). This is a steady-state two-level (centered at 250-hPa and 750-hPa) primitive equation model, linearized about a prescribed background mean state. The formulation is similar to that of the multilevel linear baroclinic model used by Hoskins and Simmons (1975) and others, but its governing equations are greatly simplified by employing Gill's (1980) simple thermodynamic equation. The simple model captures three fundamental dynamic processes: (1) a heating-induced baroclinic mode as

described by the Matsuno-Gill model (Matsuno 1966; Gill 1980); (2) a barotropic Rossby wave source resulting from conversion of the heating-induced baroclinic mode into barotropic anomalies; and (3) teleconnections to high latitudes, as in the barotropic stationary wave model of Branstator (1983). For the detail on this model, see Lee et al. (2009) or Wang et al. (2010).

## 3. Classification of El Niño Modoki I and II

The correlation maps in Fig. 1 suggest that the rainfall anomalies in southern China during fall and winter are positively related to canonical El Niño, but not to El Niño Modoki. Do the correlation maps represent the true rainfall relationships with El Niño? To further examine the rainfall relationships, we first define the years of canonical El Niño and El Niño Modoki. As in other studies and by the Japan Meteorological Agency (e.g., Wang et al. 2009), canonical El Niño is defined by the Nino3 SST anomalies such that the 5-month running mean Nino3 SST anomalies are +0.5ºC or higher for six consecutive months or longer. According to this definition, twelve canonical El Niño events in the period of 1910-2010 can be identified: 1911/12, 1918/19, 1925/26, 1930/31, 1951/52, 1957/58, 1965/66, 1972/73, 1976/77, 1982/83, 1986/87, and 1997/98. Several methods have been proposed to define El Niño Modoki which is also referred to the Central-Pacific (CP) El Niño (Kao and Yu 2009; Yu and Kim 2010), or Date Line El Niño (Larkin and Harrison 2005), or Warm Pool El Niño (Kug et al. 2009) [see the recent ENSO review by Wang et al. (2013)]. Kao and Yu (2009) and Yu and Kim (2010) obtain the CP El Niño pattern by first removing the portion of the tropical Pacific SST anomalies that are regressed with the Nino1+2 SST index and then applying an empirical orthogonal function analysis to the residual SST anomalies. The regression with the Nino1+2 index is considered as an estimate of the influence of the eastern Pacific El Niño, which should be removed to better

reveal the SST anomalies associated solely with the CP El Niño. They identify the CP El Niño events during the second half of the 20th century, which agree with those identified by using other El Niño Modoki indices (Ashok et al. 2007; Ren and Jin 2011). If we extend this classification back to the early 20th century, we can identify seventeen El Niño Modoki events: 1914/15, 1923/24, 1940/41, 1941/42, 1963/64, 1968/69, 1977/78, 1979/80, 1987/88, 1990/91, 1991/92, 1992/93, 1993/94, 1994/95, 2002/03, 2004/05, and 2009/10.

We then plot the time series of the rainfall anomalies in southern China (107°E-120°E, 24°N-30°N) during fall (September to November, SON) with the canonical El Niño and El Niño Modoki years marked, as shown in Fig. 2. Of these canonical El Niño events, seven (1911/12, 1951/52, 1965/66, 1972/73/ 1976/77, 1982/83, and 1997/98) are associated with the rainfall anomalies larger than +0.5 standard deviation. The exception occurs during the 1920s/30s when the decadal forcing cancels the effect of El Niño (Chan and Zhou 2005), resulting in the smaller rainfall anomalies varying between ±0.5 standard deviation during that period. For 1986/1987 El Niño, the Nino3 index began warming (exceeding 0.5°C) in November 1986, and thus it weakly influenced southern China precipitation during fall of 1986. The rainfall anomaly for the 1957/58 El Niño was marginally smaller than +0.5 standard deviation. These results are consistent with the correlation in Fig. 1 that the rainfall anomalies in southern China during fall are positively correlated with the Nino3 index of canonical El Niño.

However, the situation is different for the case of El Niño Modoki. Among the seventeen El Niño Modoki events, seven El Niño Modoki events of 1914/15, 1940/41, 1941/42, 1963/1964, 1987/88, 1990/91, and 2002/03 are associated with the largely (larger than +0.5 standard deviation) positive rainfall anomalies in southern China, whereas six El Niño Modoki events of 1968/69, 1979/80, 1991/92, 1992/93, 2004/05, and 2009/10 correspond to the largely negative

rainfall anomalies. In the other four El Niño Modoki years of 1923/24, 1977/78, 1993/94, and 1994/95, the rainfall anomalies in southern China are small and vary between ±0.5 standard deviation. These positive and negative rainfall anomalies result in insignificant correlation between the rainfall anomalies in southern China and EMI index during fall, as shown in Fig. 1.

We also examine the relationship of southern China rainfall with El Niño Modoki in winter of the El Niño mature year. We found that nine El Niño Modoki years are associated with positive rainfall anomalies larger than +0.5 standard deviation, whereas three El Niño Modoki years correspond to negative rainfall anomalies below -0.5 standard deviation (not shown). These indicate that the feature of the opposite rainfall anomalies in southern China during winter of El Niño Modoki is weaker. In this paper, we focus on fall of the El Niño developing year.

The relationships between El Niño and rainfall in southern China are much clearer if we calculate rainfall anomaly composites (Fig. 3). During fall of canonical El Niño (Fig. 3a), the significantly positive and negative rainfall anomalies are observed in southern and northern China, respectively, which is consistent with previous results (Wang et al. 2000; Wu et al. 2003; Zhang et al. 2011). If all seventeen El Niño Modoki events are used to calculate the rainfall composite, the significant positive rainfall anomalies in southern China disappear (Fig. 3b). As demonstrated in Fig. 2, the rainfall anomalies in southern China are significantly negative for some years of El Niño Modoki and positive for other years of El Niño Modoki. That is, the rainfall anomalies in southern China cancel each other. If we use the half standard deviation of the rainfall anomalies in southern China as a threshold, we can identify seven years of El Niño Modoki (1914/15, 1940/41, 1941/42, 1963/1964, 1987/88, 1990/91, and 2002/03) when rainfall in southern China is largely increased and six years (1968/69, 1979/80, 1991/92, 1992/93, 2004/05, and 2009/10) when rainfall is significantly decreased. For the case of seven years in

Fig. 3c, the spatial rainfall anomaly patterns are similar to canonical El Niño. However, for the case of six years in Fig. 3d, the rainfall anomalies in southern China are opposite to those of Fig. 3c and canonical El Niño (Fig. 3a). The positive and negative rainfall anomaly patterns are expected because Figs. 3c and 3d are constructed and composited based on the time series of the rainfall anomalies in southern China in Fig. 2 by identifying two groups of El Niño Modoki events. As shown later, these two groups of El Niño Modoki events are also associated with different anomalous SST and atmospheric circulation patterns. We thus call and name these two groups of El Niño Modoki as El Niño Modoki I and II.

## 4. Evolution of SST anomaly patterns of various El Niño events

El Niño events occur irregularly with a timescale of 2-7 years. However, each of El Niño events follows a similar evolution of starting in spring, developing in summer/fall, and maturing in winter (e.g., Rasmusson and Carpenter 1982). Because of this, oceanographers and meteorologists usually calculate and derive El Niño composites for better understanding of the evolving nature of El Niño. Here we composite the evolution of SST anomalies for various types of El Niño events from the onset phase to the mature phase (Fig. 4). For canonical El Niño (the first column of Fig. 4), the warm SST anomalies first appear along the South American coast in boreal spring and then propagate westward (Rasmusson and Carpenter 1982). Due to the Bjerknes' positive feedback, the warm SST anomalies are further intensified and reach a maximum in winter with the largest values in the equatorial eastern Pacific. The cold SST anomalies develop in the off-equatorial western Pacific, especially during and after the mature phase of El Niño (Weisberg and Wang 1997; Wang et al. 1999; Wang and Weisberg 2000).

However, for El Niño Modoki the warm SST anomalies do not originate from the South American coast. For the group of El Niño Modoki I (the second column of Fig. 4), the warm SST anomalies are seen over the equatorial central Pacific in spring. Then, the warm SST anomalies gradually intensify and peak in the central Pacific during winter. For El Niño Modoki II (the third column of Fig. 4), the warm SST anomalies first appear in the subtropical northeastern Pacific in spring and then further develop reaching the equatorial central Pacific. The SST anomaly pattern in El Niño Modoki II resembles the Pacific meridional mode shown by Chiang and Vimont (2004), which can potentially affect the onset of ENSO involved the extratropical atmospheric variability (Chang et al. 2007). It is noted that the maximum of SST anomalies over the subtropical northeastern Pacific in El Niño Modoki II appears in fall, which is distinct from the peak anomaly season of boreal spring in the Pacific meridional mode (Chiang and Vimont 2004). The difference between El Niño Modoki I and II is that the warm SST anomalies are relatively symmetric about the equator for El Niño Modoki I (similar to canonical El Niño), whereas the warm SST anomalies for El Niño Modoki II are asymmetric with the maximum SST anomalies extending and tilting from the northeastern Pacific to the equatorial central Pacific. For four years of El Niño Modoki with small rainfall anomalies in southern China (1923/24, 1977/78, 1993/94, and 1994/95), both the SST anomaly origin and pattern are a mixture of those for El Niño Modoki I and II (not shown).

If we compare the SST anomaly spatial patterns between El Niño Modoki I and II during fall of the El Niño developing year (the season that the present paper focuses on), we note two differences. First, the warm SST anomalies are symmetric about the equator for El Niño Modoki I, whereas the warm SST anomalies are north of the equator for El Niño Modoki II. Second, the positive SST anomalies in the equatorial central Pacific extend further westward (about 10° in

longitude) for El Niño Modoki II than El Niño Modoki I. These SST anomaly differences as well as the different origins induce different atmospheric circulation patterns (as shown in next two sections) which in turn contribute to different impacts on rainfall anomalies in southern China and typhoon landfall activity.

## 5. Mechanisms of southern China rainfall anomalies for various El Niño events

Previous sections have shown that El Niño Modoki I and II have different SST anomaly distributions and different rainfall impacts in southern China. A natural question is: What are mechanisms of the rainfall anomalies in southern China associated with various El Niño events? To answer this question, we calculate composites of sea level pressure (SLP) and 850-hPa wind anomalies for canonical El Niño, El Niño Modoki I and El Niño Modoki II (Fig. 5). A common feature for all of these El Niño events is that the SLP anomalies display a see-saw pattern between the western and eastern Pacific although the amplitudes of the SLP anomalies for canonical El Niño, El Niño Modoki I and El Niño Modoki II are different, reflecting a fundamental feature of the Southern Oscillation as found by Sir Gilbert Walker in the 1920s (Walker 1923). Another feature is that all El Niño events are characterized by equatorial westerly wind anomalies, but the locations of the westerly wind anomalies for El Niño Modoki I and II are located further westward.

However, the atmospheric circulations in the western Pacific and over East Asia show different patterns for various El Niño events. For canonical El Niño, an anomalous anticyclone resides near the Philippine Sea (Fig. 5a), consistent with previous studies that emphasized the importance of the ENSO western Pacific anomaly patterns (Weisberg and Wang 1997; Wang et al. 1999; Wang et al. 2000). This anomalous anticyclone produces southwesterly wind

anomalies along the coast of southern and eastern China that carry moisture to southern China for rainfall there. For El Niño Modoki I, the anomalous anticyclone is weaker, but is still located near the Philippines (Fig. 5b). However, for El Niño Modoki II, an anomalous cyclone is just east of the Philippines (Fig. 5c). A careful comparison of Figs. 5a and c suggests that the atmospheric circulation patterns for El Niño Modoki II are a westward shift of those for canonical El Niño. For the case of El Niño Modoki II, an anomalous anticyclone moves westward to southern East Asia. The anomalous cyclone east of the Philippines in Fig. 5c reflects Gill's (1980) response to the warm SST anomalies in the equatorial central Pacific (more details are shown in next section). Thus, the wind anomalies in southern China for El Niño Modoki II are northerly, which supply the dry air and thus are unfavorable for rainfall.

We further calculate the moisture flux and its divergence anomalies for canonical El Niño, El Niño Modoki I and El Niño Modoki II during fall of the El Niño developing year (Fig. 6). For both canonical El Niño and El Niño Modoki I, southern (northern) China is associated with anomalous moisture convergence (divergence) (Figs. 6a and b). However, the moisture divergence pattern in China for El Niño Modoki II is opposite to that of canonical El Niño and El Niño Modoki I (Fig. 6c). Both of these moisture flux and moisture divergence distributions are consistent with and explain the rainfall anomaly composites in China (Fig. 3).

We also calculate composites of 500-hPa pressure vertical velocity anomalies for canonical El Niño, El Niño Modoki I and El Niño Modoki II during fall of the El Niño developing year (Fig. 7). All El Niño events show anomalous ascending motion in the equatorial eastern and central Pacific, reflecting the fundamental physics of SST-induced atmospheric deep convection associated with El Niño events. For canonical El Niño and El Niño Modoki I, southern China is characterized by anomalous upward motion, indicating enhanced convection

and the tendency for increased rainfall. However, for El Niño Modoki II, southern and eastern China features anomalous downward motion, suppressing convective activity and thus decreasing rainfall. Again, these results are consistent with the rainfall composites in Fig. 3. Since the atmospheric reanalysis products and the GPCC rainfall data are independent, the consistency suggests that the results are robust.

## 6. Model results

The simple atmospheric model described in Section 2 is used to examine the response to SST anomalies. The composited SST anomalies during fall for canonical El Niño, El Niño Modoki I and El Niño Modoki II (Fig. 4) are used to force the model. The model results for the baroclinic streamfunction are shown in Fig. 8. A common feature is that in response to a warm heating anomaly in the equatorial eastern and central Pacific, the baroclinic streamfunction from the model experiments shows a pair of cyclones straddled on the equator (the left panels of Fig. 8). This is indicative that Gill's (1980) dynamics are at work: the equatorial warm SST anomalies produce a pair of cyclones north and south of the equator which in turn induces equatorial westerly wind anomalies to the west of the heating region. The pair of cyclones for El Niño Modoki events is further westward than canonical El Niño event, consistent with the observed wind distribution patterns associated with various El Niño events (Fig. 5).

The model response in the tropical western North Pacific is also basically consistent with the observational results shown in the previous sections. For the model experiment of canonical El Niño, a strong anticyclone is located in the north of the Philippines. For El Niño Modoki I and II, a weak anticyclone resides over Asia. In particular, the model experiment of El Niño Modoki II shows that the cyclone is extended westward to the east of the Philippine Sea and

Indonesia, consistent with the observed result in Fig. 5c. We also perform the additional model experiments by removing the forcings of the negative SST anomalies in the western Pacific (the right panels of Fig. 8). For the case of canonical El Niño, the anticyclone north of the Philippines disappears (Fig. 8d). For the model experiments of El Niño Modoki, the cyclones extend westward reaching the east coast of China. These indicate that the atmospheric circulation in the tropical western North Pacific is controlled by local cold SST anomalies and warm SST anomalies in the equatorial central and eastern Pacific associated with various El Niño events.

## 7. Influence of various El Niño events on the typhoon tracks

Since canonical El Niño, El Niño Modoki I and El Niño Modoki II are associated with different atmospheric circulation patterns in the western North Pacific and over East Asia, we expect that these various El Niño events can affect the typhoon or tropical cyclone (TC) tracks in the western North Pacific. From 1950 to 2010, El Niño events feature six years of canonical El Niño (1951/52, 1965/66, 1972/73/ 1976/77, 1982/83, and 1997/98), four years of El Niño Modoki I (1963/64, 1987/88, 1990/91, and 2002/03) and six years of El Niño Modoki II (1968/69, 1979/80, 1991/92, 1992/93, 2004/05, and 2009/10). Figure 9 shows the typhoon (categories 1-5) tracks for these El Niño events during fall of the El Niño developing year. The average numbers of typhoons during fall of canonical El Niño, El Niño Modoki I and El Niño Modoki II are 5.7, 5.5 and 7.2 per year, respectively. The number of typhoons per year for El Niño Modoki II is slightly larger than canonical El Niño and El Niño Modoki I. However, the ratios of China landfalling typhoons (i.e., the number of landfalling divided by the total number of typhoons) are respectively 18%, 27%, and 9% for canonical El Niño, El Niño Modoki I and El

Niño Modoki II. That is, the landfalling ratio for El Niño Modoki II is two or three times smaller than those for canonical El Niño and El Niño Modoki I. In other words, El Niño Modoki II is not favorable for the northwestward track of typhoons in the western North Pacific. [Note that previous studies have classified three prevailing typhoon tracks in the western North Pacific: (1) the westward track across the Philippines and the South China Sea to Vietnam, (2) the northwestward track toward the south and east coast of China, and (3) the recurving track toward the regions near Japan and the sea east of Japan (e.g., Liu and Chan 2008).]

In the tropical western North Pacific, TCs usually move toward the west with a slight poleward component due to an axis of high pressure called the western North Pacific subtropical high (WNPSH) that extends east-west poleward of TCs. On the equatorward side of the WNPSH, the easterly trade winds prevail. However, if the WNPSH is weak and/or shifts eastward, TCs may turn poleward and then recurve toward the east as in the case of hurricanes in the North Atlantic (e.g., Liu and Fearn 2000; Elsner et al. 2000; Wang et al. 2011). On the poleward side of the WNPSH, the westerly winds prevail thus steering TCs back to the east. Hence, the position and strength of the WNPSH can determine and change the movement of TCs. We calculate the composites of the WNPSH for canonical El Niño, El Niño Modoki I and El Niño Modoki II during fall of the El Niño developing year (Fig. 10). For both canonical El Niño and El Niño Modoki I, the WNPSH extends westward to the South China Sea and even to southern East Asia. However, for the case of El Niño Modoki II, the WNPSH shifts slightly eastward in comparison with the WNPSH climatological position (Fig. 10c). Thus, the eastward shift of the WNPSH will allow a more frequent northeastward recurvature of typhoons, whereas the westward shift of the WNPSH creates a more favorable condition for typhoons to make landfall. In other words, El Niño Modoki II does not allow the WNPSH to extend far west,

meaning that typhoons likely would be steered around WNPSH's edge to the northeast instead of making landfall in China.

In fact, the movement of TCs is mainly steered by the surrounding environmental flow in the troposphere and modified by the beta-effect. An integrated flow through a layer of the atmosphere is usually defined as the TC steering flow (e.g., Dong and Neumann 1986; Velden and Leslie 1991). The steering flow patterns associated with canonical El Niño, El Niño Modoki I and El Niño Modoki II during fall of the El Niño developing year are shown in Fig. 11. As in the rainfall influence, canonical El Niño and El Niño Modoki I share a similar pattern of the TC steering flow with the southwesterly anomalies in the south coast of China and the west of the Philippines. However, for the case of El Niño Modoki II, the northwesterly anomalies of the TC steering flow blow in the south coast of China, the South China Sea and the Philippine Sea (Fig. 11c), which are unfavorable for typhoons to make landfall in China. The differences of the TC steering flow explain why El Niño Modoki II has a smaller ratio or number of typhoons making landfall in China compared to canonical El Niño and El Niño Modoki I.

## 8. Summary and discussion

El Niño is characterized by interannual, large-scale and warm SST variations in the equatorial eastern-to-central Pacific. Canonical El Niño and El Niño Modoki exhibit maximum warm SST anomalies in the equatorial eastern and central Pacific, respectively, and have different climate impacts [see the recent review by Wang et al. (2013)]. The present paper uses observational data to show the different impacts of various El Niño events on rainfall in southern China and the typhoon tracks in the western North Pacific. Based on the opposite influence on rainfall in southern China during fall of the El Niño developing year, we identify two groups of

El Niño Modoki events: El Niño Modoki I and II. El Niño Modoki I and II show the different origins and patterns of SST anomalies. The warm SST anomalies first appear in the equatorial central Pacific for El Niño Modoki I, whereas they originate from the subtropical northeastern Pacific for El Niño Modoki II. Thus, during fall of the El Niño developing year, El Niño Modoki I shows a symmetric SST anomaly distribution about the equator with the maximum warming in the central Pacific. However, El Niño Modoki II displays an asymmetric SST anomaly distribution, with the warm SST anomalies extending and tilting from the subtropical northeastern Pacific to the equatorial central Pacific. In addition, the positive SST anomalies in the equatorial central Pacific extend further westward for El Niño Modoki II than El Niño Modoki I.

Corresponding to various El Niño events are different atmospheric circulation patterns in the western North Pacific and East Asia during fall of the El Niño developing year. Similar to canonical El Niño, El Niño Modoki I is accompanied by an anomalous anticyclone in the Philippine Sea although the anticyclone is weaker than that of canonical El Niño. The anomalous anticyclone produces southwesterly wind anomalies along the south coast of China, inducing moisture convergence conducive to enhanced rainfall in southern China. However, for El Niño Modoki II, an anomalous cyclone resides east of the Philippines, which corresponds to northerly wind anomalies near the south coast of China and thus produces moisture divergence that tends to decrease rainfall in southern China. Simple atmospheric model experiments show that the atmospheric circulation patterns in the tropical western North Pacific are controlled by local cold SST anomalies in the western Pacific and warm SST anomalies in the equatorial central and eastern Pacific associated with various El Niño events. The anomalous cyclone east

of the Philippines for El Niño Modoki II is due to the further westward extension of the warm central Pacific SST anomalies observed for El Niño Modoki II.

We have to point out that these atmospheric anomalous circulation patterns during fall of the El Niño year do not seem to apply to winter of the El Niño year. During winter of the El Niño year (i.e., the mature phase of El Niño), all of the canonical El Niño, El Niño Modoki I and II show an anomalous anticyclone near the Philippines although there are some differences in the amplitude and locations (not shown). For all cases, the southwesterly wind anomalies blow along the coast of southern China, in spite of the weak wind anomalies associated with El Niño Modoki II. These are consistent with the winter rainfall distributions in southern China. As in fall, canonical El Niño is associated with the positive rainfall anomalies in southern China during winter. However, the feature of the opposite rainfall anomalies in southern China for El Niño Modoki I and II is weak during winter. Among the El Niño Modoki events from 1910-210, nine El Niño Modoki years are associated with positive winter rainfall anomalies larger than +0.5 standard deviation, whereas three El Niño Modoki years correspond to the negative winter rainfall anomalies below -0.5 standard deviation (not shown).

Various El Niño events also show different influences on the western North Pacific subtropical high (WNPSH). Canonical El Niño and El Niño Modoki I are associated with a westward extension of the WNPSH, whereas El Niño Modoki II shifts the WNPSH eastward in comparison with its climatological position. Not surprisingly, associated with the east-west shifts of the WNPSH are different impacts on the TC tracks in the western North Pacific because the movement of TCs is mainly steered by the surrounding environmental flow in the atmosphere and modified by the beta-effect. In contrast to canonical El Niño and El Niño Modoki I, El Niño Modoki II is associated with the northwesterly anomalies of the TC steering flow which are

unfavorable for typhoons to make landfall in China. In other words, El Niño Modoki II induces a TC steering flow pattern which decreases the possibility for typhoons to make landfall in China. Note that we calculate the sensitivity of the TC steering flow to the layer of the atmosphere used to define the steering flow. All calculations show the northwesterly anomalies of the TC steering flow for El Niño Modoki II, indicating that the unfavorable TC steering flow anomalies are a robust result for El Niño Modoki II.

In this paper, the WNPSH is represented by the contour of 5864 gpm of the 500-hPa geopotential height. Although the position of the WNPSH is sensitive to the selection of contour lines, the basic feature of the zonal shifts for canonical El Niño, El Niño Modoki I, and El Niño Modoki II does not depend upon the contour selections. We also choose other contour lines such as that of Sui et al. (2007) and we obtain the similar results. That is, canonical El Niño and El Niño Modoki I are associated with a westward extension of the WNPSH, whereas El Niño Modoki II corresponds to an eastward shift. However, the physics of the zonal shifts of the WNPSH for various El Niño events need to be investigated given that the formation mechanisms of the subtropical highs are in debate and many hypotheses have been proposed (e.g., Rodwell and Hoskins 2001; Seager et al. 2003; Liu and Wu 2004; Liu et al. 2004; Miyasaka and Nakamura 2005; Nigam and Chan 2009). In addition, it is not clear why the westward extension of the WNPSH for El Niño Modoki I is larger than that of canonical El Niño (Fig. 10).

Why various El Niño events show the different origins of SST anomalies is unknown. For canonical El Niño, the warm SST anomalies first appear along the South American coast in boreal spring and then propagate westward (e.g., Rasmusson and Carpenter 1982) reaching the maximum warming in the equatorial eastern Pacific. For El Niño Modoki I, the warm SST anomalies are seen over the equatorial central Pacific in spring and then gradually intensify and

reach the maximum in the equatorial central Pacific. For El Niño Modoki II, the warm SST anomalies originate in the subtropical northeastern Pacific in spring and then further develop reaching the equatorial central Pacific. These different origins of SST anomalies may be associated with different ENSO mechanisms such as the recharge-discharge oscillator (Jin 1997) or other oscillators [see the review by Wang and Picaut (2004)] for canonical El Niño, and possible mechanisms of the zonal advection feedback (e.g., Kug et al. 2009), the subtropical connections (Yu et al. 2010; Yu and Kim 2011) and the seasonal footprinting (Vimont et al. 2003; Chang et al. 2007) for El Niño Modoki events.

Yeh et al. (2009) compared the ratio of El Niño Modoki events to canonical El Niño events in the Coupled Model Intercomparison Project phase 3 (CMIP3) model simulations and noticed that the ratio is projected to increase under a global warming scenario. Their study suggests that El Niño Modoki may become the dominant El Niño type in a future warmer climate. Our study suggests that we need to examine the relative changes of El Niño Modoki I and II under global warming. This may be an important issue since it will tell us the variations of rainfall in southern China and typhoon landfall activity in a warmer climate.

*Acknowledgments*. We thank two anonymous reviewers and Dr. Greg Foltz for their comments and suggestions on the manuscript. This work was supported by grants from National Oceanic and Atmospheric Administration (NOAA) Climate Program Office and the base funding of NOAA Atlantic Oceanographic and Meteorological Laboratory (AOML). The findings and conclusions in this report are those of the author(s) and do not necessarily represent the views of the funding agency.

## References


Ashok, K., S. K. Behera, S. A. Rao, H. Weng, and T. Yamagata, 2007: El Niño Modoki and its possible teleconnection. *J. Geophys. Res.*, **112**, C11007, doi:10.1029/2006JC003798.

Branstator, G., 1983: Horizontal energy propagation in a barotropic atmosphere with meridional and zonal structure. *J. Atmos. Sci.*, **40**, 1689-1708.

Cai, W., and T. Cowan, 2009: La Niña Modoki impacts Australia autumn rainfall variability. *Geophys. Res. Lett.*, **36**, L12805, doi:10.1029/2009GL037885.

Chan, J. C. L., and W. Zhou, 2005: PDO, ENSO and the early summer monsoon rainfall over south China. *Geophys. Res. Lett.*, **32**, L08810, doi:10.1029/2004GL022015.

Chang, C.-P., Y. Zhang, and T. Li, 2000: Interannual and interdecadal variations of the East Asian summer monsoon and tropical Pacific SSTs. Part I: Rolse of the subtropical ridge. *J. Climate*, **13**, 4310-4325.

Chang, P., and Co-authors, 2007: Pacific meridional mode and El Niño-Southern Oscillation. *Geophys. Res. Lett.*, **34**, L16608, doi:10.1029/2007GL030302.

Chiang, J. C. H., and D. J. Vimont, 2004: Analogous Pacific and Atlantic meridional modes of tropical atmosphere-ocean variability. *J. Climate*, **17**, 4143-4158.

Compo, G. P., and Co-authors, 2011: The Twentieth Century Reanalysis Project. *Quart. J. Roy. Meteor. Soc.,* **137**, 1-28.

Dong, K., and C. J. Neumann, 1986: The relationship between tropical cyclone motion and the environmental geostrophic flows. *Mon. Weather Rev.*, **114**, 115-122.

Elsner, J. B., K. Liu, and B. Kocher, 2000: Spatial variations in major U.S. hurricane activity: Statistics and a physical mechanism. *J. Climate*, **13**, 2293-2305.

Feng, J., and J. Li, 2011: Influence of El Niño Modoki on spring rainfall over south China. *J. Geophys. Res.*, **116**, D13102, doi:10.1029/2010JD015160.

Feng, J., W. Chen, C.-Y. Tam and W. Zhou, 2011: Different impacts of El Niño and El Niño Modoki on China rainfall in the decaying phases. *Int. J. Climatol.*, **31**, 2091-2101.

Gill, A. E., 1980: Some simple solutions for heat-induced tropical circulation. *Quart. J. Roy. Meteor. Soc.*, **106**, 447-462.

Hoskins, B. J. and A. J. Simmons, 1975: A multi-layer spectral model and the semi-implicit method. *Quart. J. Roy. Meteor. Soc.*, **103**, 553-567.

Huang, R., and Y. Wu, 1989: The influence of ENSO on the summer climate change in China and its mechanism. *Adv. Atmos. Sci.,* **6**, 21-32.

Jin, F.-F., 1997: An equatorial ocean recharge paradigm for ENSO. Part I: Conceptual model. *J. Atmos. Sci.,* **54**, 811-829.

Kalnay, E., and Co-authors, 1996: The NCEP/NCAR 40-year reanalysis project. *Bull. Am. Meteorol. Soc.*, **77**, 437-471.

Kao, H. Y., and Yu, J.-Y., 2009: Contrasting Eastern-Pacific and Central-Pacific Types of ENSO. *J. Climate*, **22**, 615-632.

Kim, H.-M., P. J. Webster, and J. A. Curry, 2011: Modulation of North Pacific tropical cyclone activity by three phases of ENSO. *J. Climate*, **24**, 1839-1849.

Kug, J.-S., F.-F. Jin, and S.-I. An, 2009: Two types of El Niño events: Cold tongue El Niño and warm pool El Niño. *J. Climate*, **22**, 1499-1515.

Larkin, N. K., and D. E. Harrison, 2005: Global seasonal temperature and precipitation anomalies during El Niño autumn and winter. *Geophys. Res. Lett.*, **32**, L16705, doi:10.1029/2005GL022860.

Lee, S.-K., C. Wang, and B. Mapes, 2009: A simple atmospheric model of the local and teleconnection responses to heating anomalies. *J. Climate*, **22**, 272-284.

Li, C., W. Zhou, X. Jia, and X. Wang, 2006: Decadal/interdecadal variations of ocean temperature and its impacts on climate. *Adv. Atmos. Sci.*, **23**, 964-981.

Liu, K.-B., and M. L. Fearn, 2000: Reconstruction of prehistoric landfall frequencies of catastrophic hurricanes in Northwestern Florida from Lake sediment records. *Quat. Res.*, **54**, 238-245.

Liu, K. S., and J. C. L. Chan, 2008: Interdecadal variability of western North Pacific tropical cyclones tracks. *J. Climate*, **21**, 4464–4476.

Liu, Y., and G. Wu, 2004: Progress in the study on the formation of the summertime subtropical anticyclone. *Adv. Atmos. Sci.*, **21**, 322-342.

Liu, Y., G. Wu, and R. Ren, 2004: Relationship between the subtropical anticyclone and diabatic heating. *J. Climate*, **17**, 682-698.

Matsuno, T., 1966: Quasi-geostrophic motions in the equatorial area. *J. Meteor. Soc. Japan*, **44**, 25-43.

Miyasaka, T., and H. Nakamura, 2005: Structure and formation mechanisms of the Northern Hemisphere summertime subtropical highs. *J. Climate*, **18**, 5046-5065.

Nigam, S., and S. C. Chan, 2009: On the summertime strengthening of the Northern Hemisphere Pacific sea-level pressure anticyclone. *J. Climate*, **22**, 1174-1192.

Rasmusson, E. M., and T. H. Carpenter, 1982: Variations in tropical sea surface temperature and surface wind fields associated with the Southern Oscillation/El Niño. *Mon. Wea. Rev.*, **110**, 354-384.

Rayner, N. A., and Co-authors, 2003: Global analysis of sea surface temperature, sea ice and night marine air temperature since the late nineteenth century. *J. Geophys. Res*., **108**, 4407, doi:10.1029/2002JD002670.

Ren, F., J. Liang, G. Wu, W. Dong, X. Yang, 2011: Reliability analysis of climate change of tropical cyclone activity over the western North Pacific. *J. Clim*., **24**, 5887–5898.

Ren, H.-L., and F.-F. Jin, 2011: Niño indices for two types of ENSO. *Geophys. Res. Lett.*, **38**, L04704, doi:10.1029/2010GL046031.

Rodwell, M. J., and B. J. Hoskins, 2001: Subtropical anticyclones and summer monsoons. *J. Climate*, **14**, 3192-3211.

Rudolf, B., H. Hauschild, W. Ruth, and U. Schneider, 1994: Terrestrial precipitation analysis: Operational method and required density of point measurements. *Global Precipitation and Climate Change*, M. Dubois and M. Desalmand, Eds., Springer-Verlag, 173–186.

Seager, R., R. Murtugudde, N. Naik, A. Clement, N. Gordon, and J. Miller, 2003: Air-sea interaction and seasonal cycle of the subtropical anticyclones. *J. Climate*, **16**, 1948-1966.

Song, J.-J., Y. Wang, and L. Wu, 2010: Trend discrepancies among three best track data sets of western North Pacific tropical cyclones. *J. Geophys. Res*., **115**, D12128. doi:10.1029/2009JD013058.

Sui, C.-H., P.-H. Chung, and T. Li, 2007: Interannual and interdecadal variability of the summertime western North Pacific subtropical high. *Geophys. Res. Lett.*, **34**, L11701, doi:10.1029/2006GL029204.

Velden, C. S., and L. M. Leslie, 1991: The basin relationship between tropical cyclone intensity and the depth of the environmental steering layer in the Australian region. *Wea. Forecasting*, **6**, 244-253.

Vimont, D. J., J. M. Wallace, and D. S. Battisti, 2003: The seasonal footprinting mechanism in the Pacific: Implications for ENSO. *J. Climate*, **16**, 2668-2675.

Walker, G. T., 1923: Correlation in seasonal variations of weather VIII: A preliminary study of world weather. *Mem. Indian Meteor. Dept.,* **24**, 75-131.

Wang, B., R. Wu, and X. Fu, 2000: Pacific–East Asian teleconnection: how does ENSO affect East Asian climate? *J. Climate,* **13**, 1517-1536.

Wang, B., and Q. Zhang, 2002: Pacific-East Asian teleconnection, part II: How the Philippine Sea anticyclone established during development of El Niño. *J. Climate*, **15**, 3252-3265.

Wang, C., R. H. Weisberg, and J. I. Virmani, 1999: Western Pacific interannual variability associated with the El Niño-Southern Oscillation. *J. Geophys. Res.*, **104**, 5131-5149.

Wang, C., and R. H. Weisberg, 2000: The 1997-98 El Niño evolution relative to previous El Niño events. *J. Climate*, **13**, 488-501.

Wang, C., and J. Picaut, 2004: Understanding ENSO physics – A review. *Earth's Climate: The Ocean-Atmosphere Interaction*. C. Wang, S.-P. Xie, and J. A. Carton, Eds., AGU Geophysical Monograph Series **147**, 21-48.

Wang, C., S.-K. Lee, and C. R. Mechoso, 2010: Inter-hemispheric influence of the Atlantic warm pool on the southeastern Pacific. *J. Climate*, **23**, 404-418.

Wang, C., H. Liu, S.-K. Lee, and R. Atlas, 2011: Impact of the Atlantic warm pool on United States landfalling hurricanes. *Geophys. Res. Lett.*, **38**, L1907, doi:10.1029/2011GL049265.

Wang, C., C. Deser, J.-Y. Yu, P. DiNezio, and A. Clement, 2013: El Niño-Southern Oscillation (ENSO): A review. In *Coral Reefs of the Eastern Pacific*. P. Glymn, D. Manzello, and I. Enochs, Eds., Springer Science Publisher, in press.

Wang, X., D. Wang, and W. Zhou, 2009: Decadal variability of twentieth-century El Niño and La Niña occurrence from observations and IPCC AR4 coupled models. *Geophys. Res. Lett.*, **36**, L11701, doi: 10.1029/2009GL037929.

Wang, X., D. Wang, W. Zhou, and C. Li, 2012: Interdecadal modulation of the influence of La Niña events on Mei-yu rainfall over the Yangtze River Valley. *Adv. Atmos. Sci.*, **29**, 157-168.

Weisberg, R. H., and C. Wang, 1997: A western Pacific oscillator paradigm for the El Niño-Southern Oscillation. *Geophys. Res. Lett*., **24**, 779-782.

Weng, H., K. Ashok, S. K. Behera, S. A. Rao, and T. Yamagata, 2007: Impacts of recent El Niño Modoki on dry/wet conditions in the Pacific rim during boreal summer. *Climate Dyn.*, **29**, 113-129.

Weng, H., S. K. Behera, and T. Yamagata, 2009: Anomalous winter climate conditions in the Pacific rim during recent El Niño Modoki and El Niño events. *Climate Dyn.*, **32**, 663-674.

Wu, R., and B. Wang, 2002: A contrast of the East Asian summer monsoon-ENSO relationship between 1962-77 and 1978-93. *J. Climate*, **15**, 3266-3279.

Wu, R., Z. Hu, and B. Kirtman, 2003: Evolution of ENSO-related rainfall anomalies in East Asia. *J. Climate*, **16**, 3742-3758.

Xie, S.-P., Y. Du, G. Huang, X. Zheng, H. Tokinaga, K. Hu, and Q. Liu, 2010: Decadal shift in El Nino influences on Indo-western Pacific and East Asian climate in the 1970s. *J. Climate,* **23**, 3352-3368.

Yeh, S.-W., J.-S. Kug, B. Dewitte, B. Kirtman, and F.-F. Jin, 2009: Recent changes in El Niño and its projection under global warming. *Nature,* **461**, 511-515.

Yu, J.-Y., and H.- Y. Kao, 2007: Decadal changes of ENSO persistence barrier in SST and ocean heat content indices: 1958-2001. *J. Geophys. Res.*, **112**, D13106, doi: 10.1029/2006JD007654.

Yu, J.-Y., and S. T. Kim, 2010: Three evolution patterns of Central-Pacific El Niño. *Geophys. Res. Lett.*, **37**, L08706, doi:10.1029/2010GL042810.

Yu, J.-Y., H.-Y. Kao, and T. Lee, 2010: Subtropics-related interannual sea surface temperature variability in the equatorial central Pacific. *J. Climate*, **23**, 2869-2884.

Yu, J.-Y., and S. T. Kim, 2011: Relationships between extratropical sea level pressure variations and Central-Pacific and Eastern-Pacific types of ENSO. *J. Climate*, **24**, 708-720.

Zhang, W., F.-F. Jin, J. Li, and H.-L. Ren, 2011: Contrasting Impacts of Two-type El Niño over the Western North Pacific during Boreal Autumn. *J. Meteor. Soc. Japan*, **89**, 563-569.

Zhou, W., and J. C. L. Chan, 2007: ENSO and the South China Sea summer monsoon onset. *Int. J. Climatol.*, **27**, 157-167.

Zhou, W., C. Li, and X. Wang, 2007a: Possible connection between Pacific Oceanic interdecadal pathway and East Asian winter monsoon. *Geophys. Res. Lett.*, **34**, L01701, doi: 10.1029/2006GL027809.

Zhou, W., X. Wang, T. Zhou, C. Li, and J. C. L. Chan, 2007b: Interdecadal variability of the relationship between the East Asian winter monsoon and ENSO. *Meteorol. Atmos. Phys.*, **98**, 283-293.

## Figure Captions

**Figure 1.** Partial correlations of rainfall anomalies with the Nino3 index and El Niño Modoki Index (EMI) during four seasons of fall (September to November; SON), winter (December to February; DJF), spring (March to May; MAM) and summer (June to August; JJA). The left panels show correlations with the Nino3 index by removing the EMI influence, and the right panels are correlations with the EMI by removing the Nino3 influence. The solid (dashed) contours represent positive (negative) correlations, with contour interval of 0.1. The zero contour line is thickened. The shadings indicate the correlation exceeding the 90% significant level.

**Figure 2.** Time series of the rainfall anomalies (mm/month) over southern China (107°-120°E, 24°-30°N) during boreal fall. The dashed lines indicate ±0.5 standard deviation. The dark dots and circles respectively represent canonical El Niño and El Niño Modoki events in the El Niño developing year.

**Figure 3.** Composites of rainfall anomalies (mm/month) during fall of the El Niño developing year for (a) canonical El Niño, (b) all events of El Niño Modoki, (c) El Niño Modoki I, and (d) El Niño Modoki II. Four panels are calculated from seven canonical El Niño years, all seventeen years of El Niño Modoki, seven years of El Niño Modoki I, and six years of El Niño Modoki II, respectively. The solid (dashed) contours represent the positive (negative) rainfall anomalies, with contour interval of 7.5 mm/month. The zero contour line is thickened. The shadings indicate the composite exceeding the 90% significant level, based on Student's *t* test.

**Figure 4.** Evolution of composited SST anomalies (°C) for canonical El Niño (the first column), El Niño Modoki I (the second column), and El Niño Modoki II (the third column). The first, second, third and fourth row represents the different El Niño phases of MAM (March[0] to May[0]), JJA (June[0] to August[0]), SON (September[0] to November[0]) and DJF (December[0] to February[+1]), respectively. The composites are calculated from seven canonical El Niño events (1911/12, 1951/52, 1965/66, 1972/73/ 1976/77, 1982/83, and 1997/98), seven El Niño Modoki I events (1914/15, 1940/41, 1941/42, 1963/1964, 1987/88, 1990/91, and 2002/03), and six El Niño Modoki II events (1968/69, 1979/80, 1991/92, 1992/93, 2004/05, and 2009/10). The white contours filled with the dots indicate the composite exceeding the 90% significant level, based on Student's *t* test.

**Figure 5.** Composites of sea level pressure (SLP) anomalies (Pa) and 850-hPa wind anomalies (m/s) for various El Niño events during fall of the El Niño developing year. Shown are for (a) canonical El Niño, (b) El Niño Modoki I and (c) El Niño Modoki II. The white contours filled with the dots indicate the SLP composite exceeding the 90% significant level, based on Student's *t* test.

**Figure 6.** Composites of moisture flux anomalies (vector; g/m/s) and moisture divergence anomalies (shading; $10^{-6}$ g/m$^2$/s) for various El Niño events during fall of the El Niño developing year. Shown are for (a) canonical El Niño, (b) El Niño Modoki I and (c) El Niño Modoki II. The moisture flux is calculated as $\vec{Q} = \int_{200mb}^{sfc} (q\vec{u}/g)dp$, where $q$ is specific humidity, $\vec{u}$ is vector

wind, $p$ is pressure, and $g$ is gravity. The white contours filled with the dots indicate the moisture divergence composite exceeding the 90% significant level, based on Student's *t* test.

**Figure 7.** Composites of 500-hPa pressure vertical velocity anomalies ($10^{-2}$ Pascal/s) for various El Niño events during fall of the El Niño developing year. Shown are for (a) canonical El Niño, (b) El Niño Modoki I and (c) El Niño Modoki II. The white contours filled with the dots indicate the composite exceeding the 90% significant level, based on Student's *t* test.

**Figure 8.** Baroclinic streamfunctions ($10^6$ $m^2/s$) from the simple model runs. The left panels show the model response to the SST anomalies (in the region of 110°E-80°W, 30°S-30°N) during fall for canonical canonical El Niño, El Niño Modoki I and El Niño Modoki II in Fig. 4. The right panels show the model response by removing the forcings of negative SST anomalies in the western Pacific. The negative (positive) streamfunction is in dashed (solid) contour. The contour interval is $2.0\times10^6$ $m^2/s$.

**Figure 9.** The typhoon tracks in the western North Pacific for various El Niño events during fall of the El Niño developing year. Shown are (a) six years of canonical El Niño (1951/52, 1965/66, 1972/73/ 1976/77, 1982/83, and 1997/98), (b) four years of El Niño Modoki I (1963/64, 1987/88, 1990/91, and 2002/03), and (c) six years of El Niño Modoki II (1968/69, 1979/80, 1991/92, 1992/93, 2004/05, and 2009/10).

**Figure 10.** Composites of the western North Pacific subtropical high (WNPSH) for various El Niño events during fall of the El Niño developing year. Shown are for (a) canonical El Niño, (b)

El Niño Modoki I and (c) El Niño Modoki II. The WNPSH is represented by the contour of 5864 gpm of the 500 hPa geopotential height. The dashed contour line represents the climatological WNPSH.

**Figure 11.** Composites of the TC steering flow anomalies ($10^3$ hPa m/s) for various El Niño events during fall of the El Niño developing year. Shown are for (a) canonical El Niño, (b) El Niño Modoki I and (c) El Niño Modoki II. The TC steering flow anomalies are computed by the vertically-averaged wind anomalies in the low troposphere from 950-hPa to 700-hPa. The red vectors indicate the wind amplitude exceeding the 90% significant level, based on Student's *t* test.

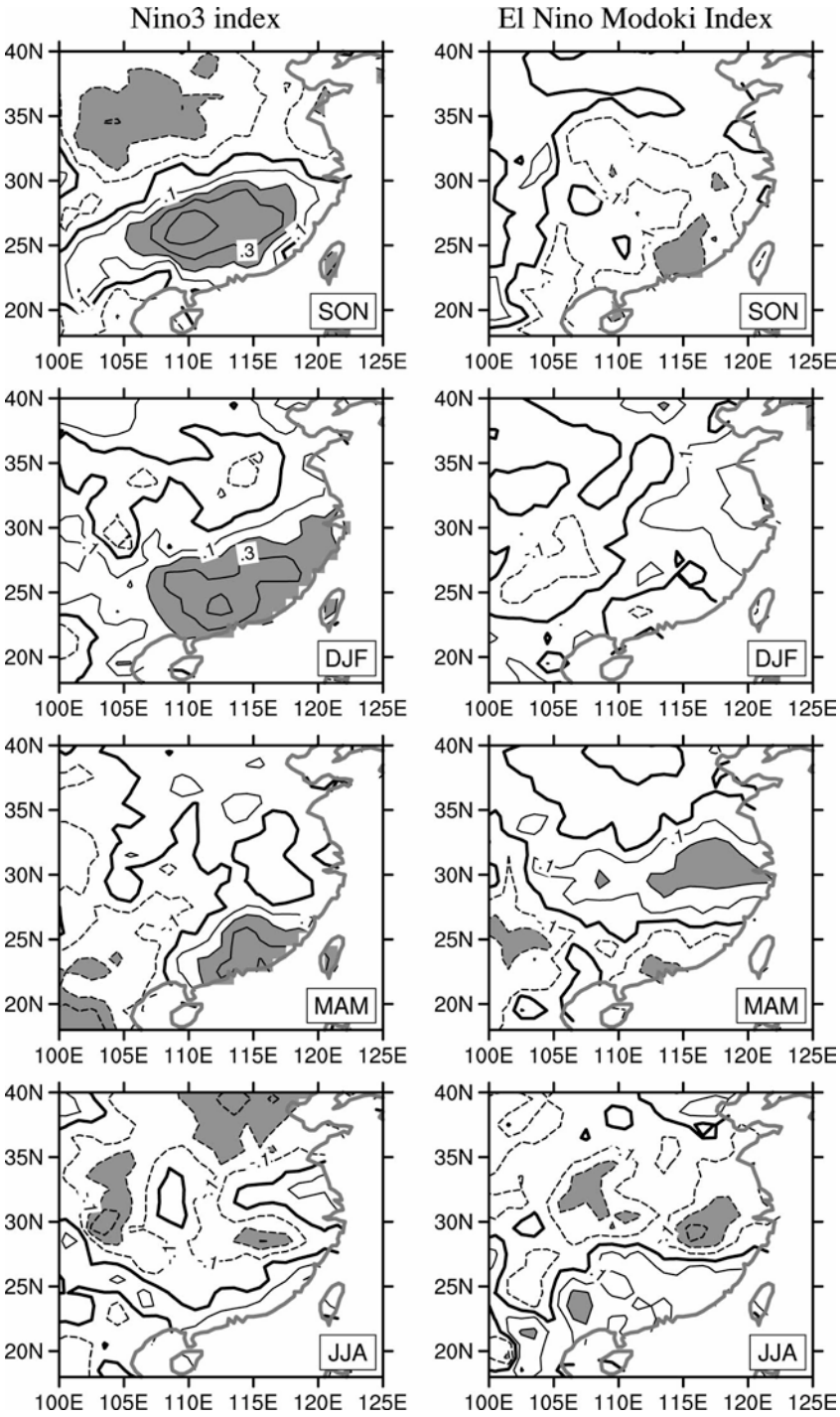


**Figure 1.** Partial correlations of rainfall anomalies with the Nino3 index and El Niño Modoki Index (EMI) during four seasons of fall (September to November; SON), winter (December to February; DJF), spring (March to May; MAM) and summer (June to August; JJA). The left panels show correlations with the Nino3 index by removing the EMI influence, and the right panels are correlations with the EMI by removing the Nino3 influence. The solid (dashed) contours represent positive (negative) correlations, with contour interval of 0.1. The zero contour line is thickened. The shadings indicate the correlation exceeding the 90% significant level.

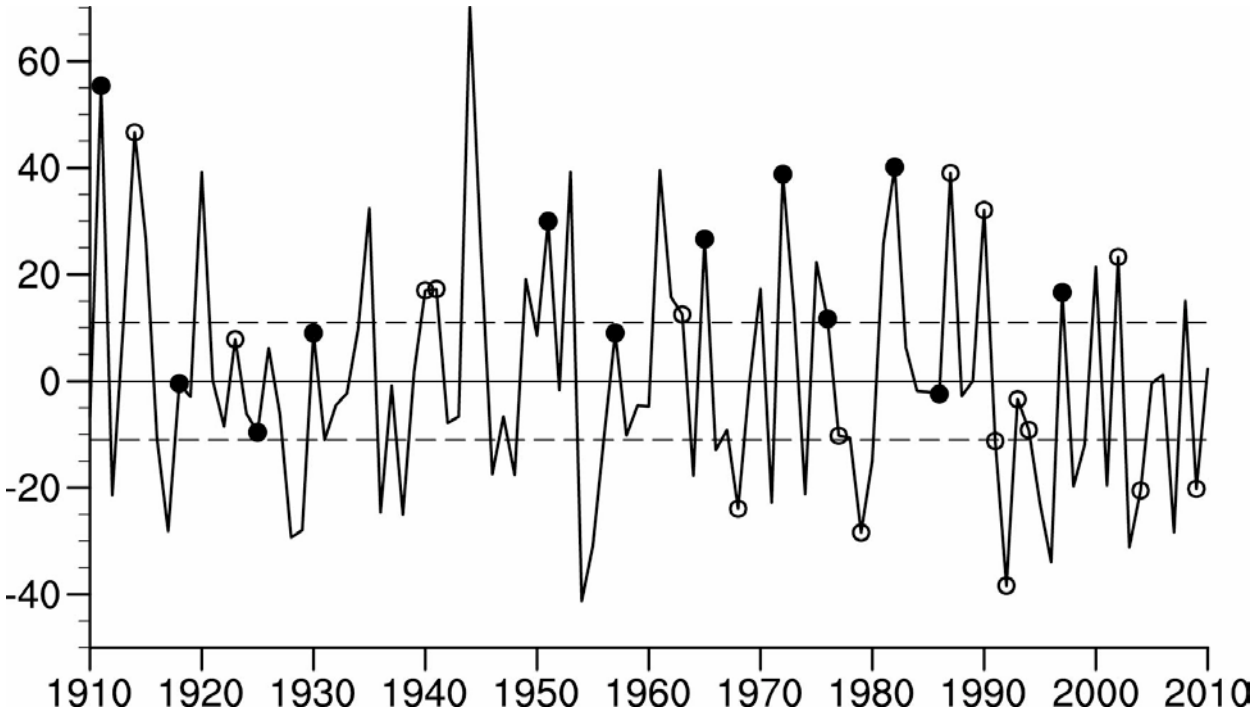


**Figure 2.** Time series of the rainfall anomalies (mm/month) over southern China (107°-120°E, 24°-30°N) during boreal fall. The dashed lines indicate ±0.5 standard deviation. The dark dots and circles respectively represent canonical El Niño and El Niño Modoki events in the El Niño developing year.

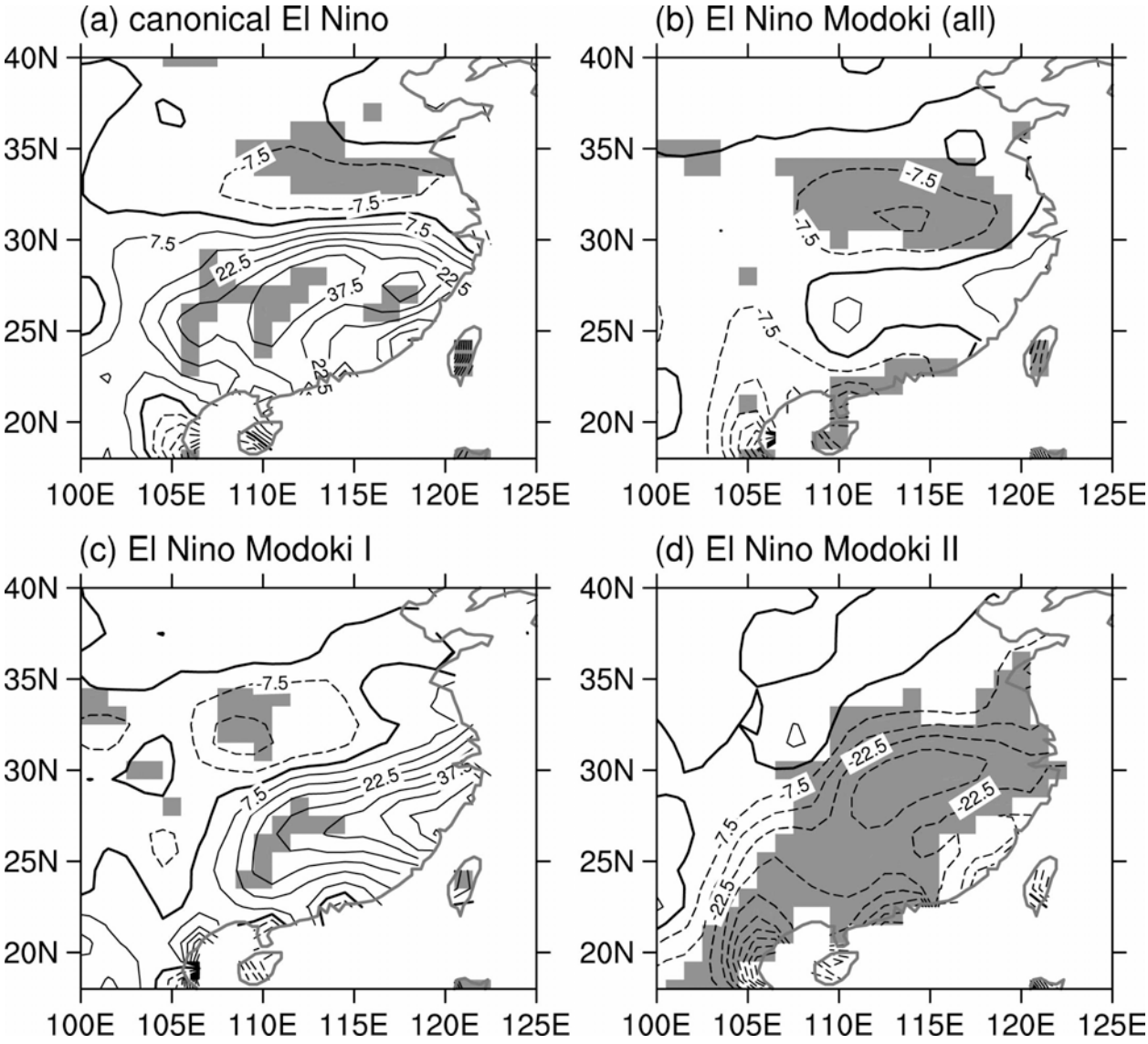


**Figure 3.** Composites of rainfall anomalies (mm/month) during fall of the El Niño developing year for (a) canonical El Niño, (b) all events of El Niño Modoki, (c) El Niño Modoki I, and (d) El Niño Modoki II. Four panels are calculated from seven canonical El Niño years, all seventeen years of El Niño Modoki, seven years of El Niño Modoki I, and six years of El Niño Modoki II, respectively. The solid (dashed) contours represent the positive (negative) rainfall anomalies, with contour interval of 7.5 mm/month. The zero contour line is thickened. The shadings indicate the composite exceeding the 90% significant level, based on Student's *t* test.

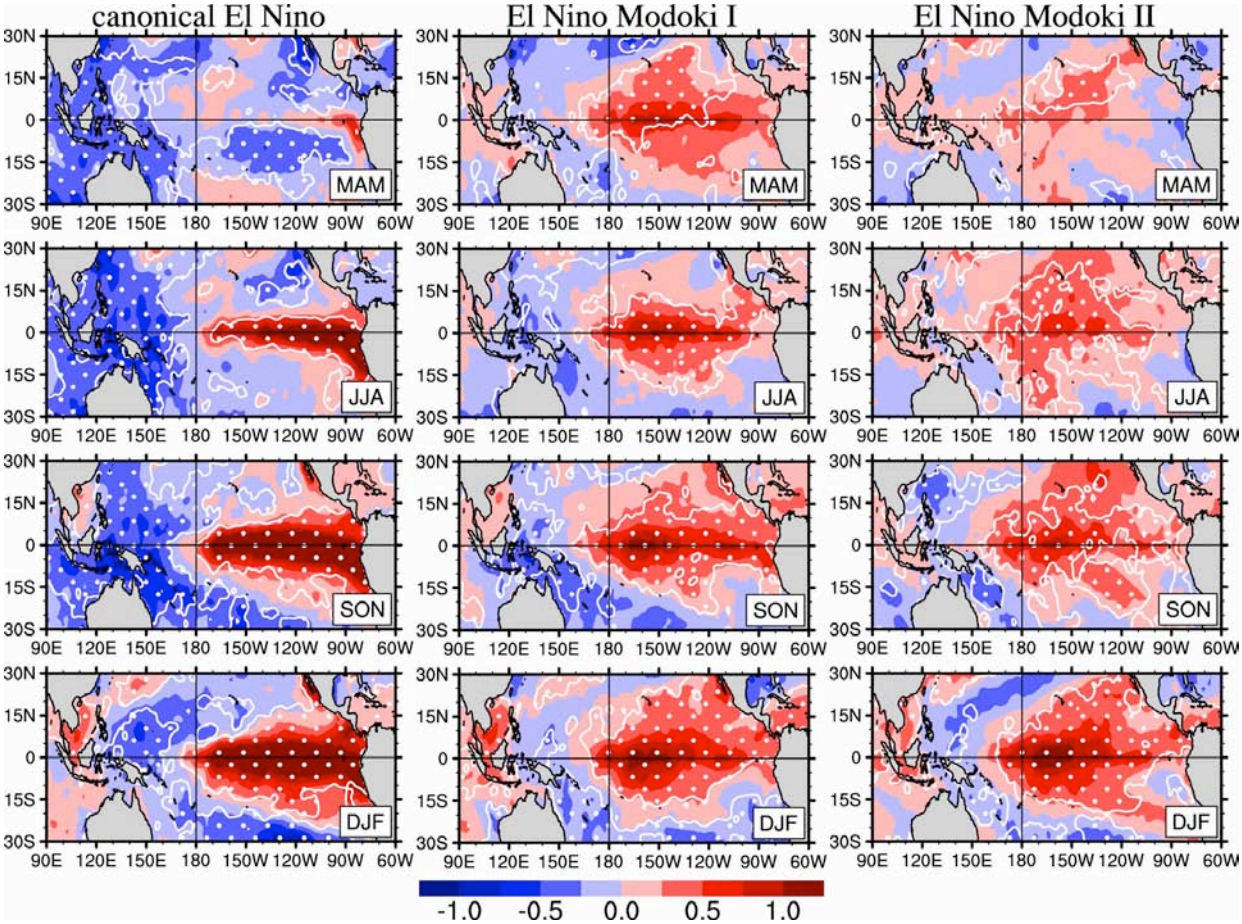


**Figure 4.** Evolution of composited SST anomalies (°C) for canonical El Niño (the first column), El Niño Modoki I (the second column), and El Niño Modoki II (the third column). The first, second, third and fourth row represents the different El Niño phases of MAM (March[0] to May[0]), JJA (June[0] to August[0]), SON (September[0] to November[0]) and DJF (December[0] to February[+1]), respectively. The composites are calculated from seven canonical El Niño events (1911/12, 1951/52, 1965/66, 1972/73/ 1976/77, 1982/83, and 1997/98), seven El Niño Modoki I events (1914/15, 1940/41, 1941/42, 1963/1964, 1987/88, 1990/91, and 2002/03), and six El Niño Modoki II events (1968/69, 1979/80, 1991/92, 1992/93, 2004/05, and 2009/10). The white contours filled with the dots indicate the composite exceeding the 90% significant level, based on Student's *t* test.

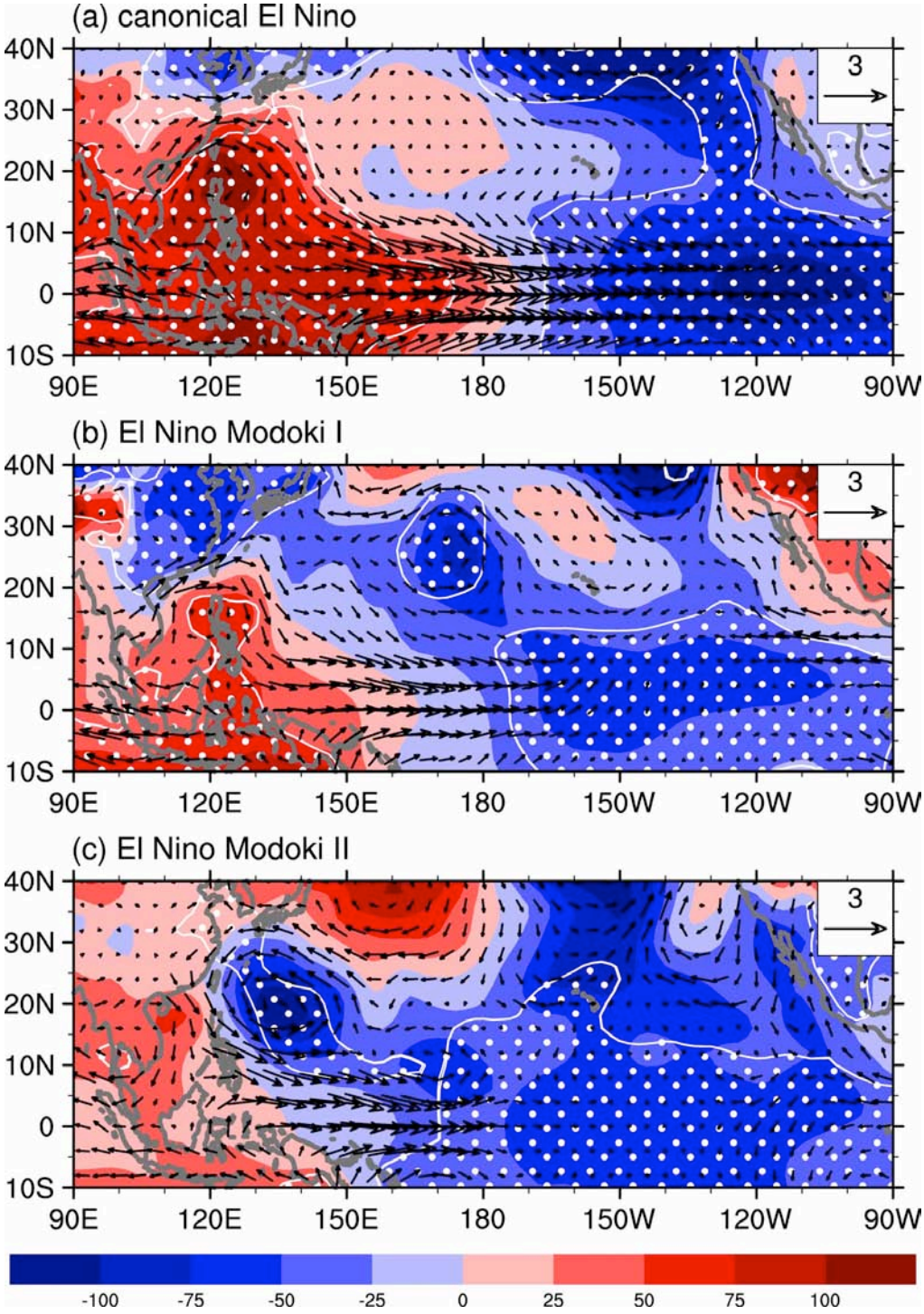


**Figure 5.** Composites of sea level pressure (SLP) anomalies (Pa) and 850-hPa wind anomalies (m/s) for various El Niño events during fall of the El Niño developing year. Shown are for (a) canonical El Niño, (b) El Niño Modoki I and (c) El Niño Modoki II. The white contours filled with the dots indicate the SLP composite exceeding the 90% significant level, based on Student's *t* test.

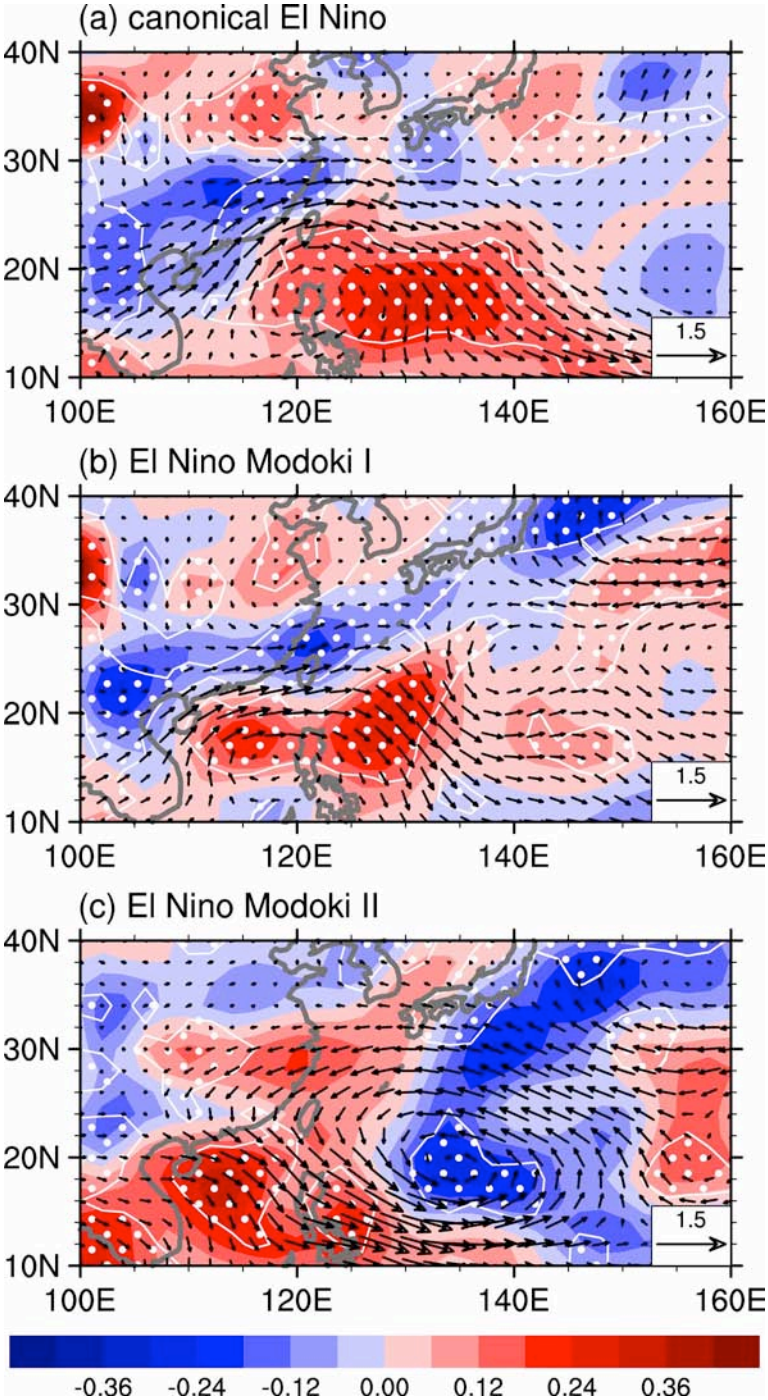


**Figure 6.** Composites of moisture flux anomalies (vector; g/m/s) and moisture divergence anomalies (shading; $10^{-6}$ g/m$^2$/s) for various El Niño events during fall of the El Niño developing year. Shown are for (a) canonical El Niño, (b) El Niño Modoki I and (c) El Niño Modoki II. The moisture flux is calculated as $\vec{Q} = \int_{200mb}^{sfc} (q\vec{u} / g) dp$, where $q$ is specific humidity, $\vec{u}$ is vector wind, $p$ is pressure, and $g$ is gravity. The white contours filled with the dots indicate the moisture divergence composite exceeding the 90% significant level, based on Student's *t* test.

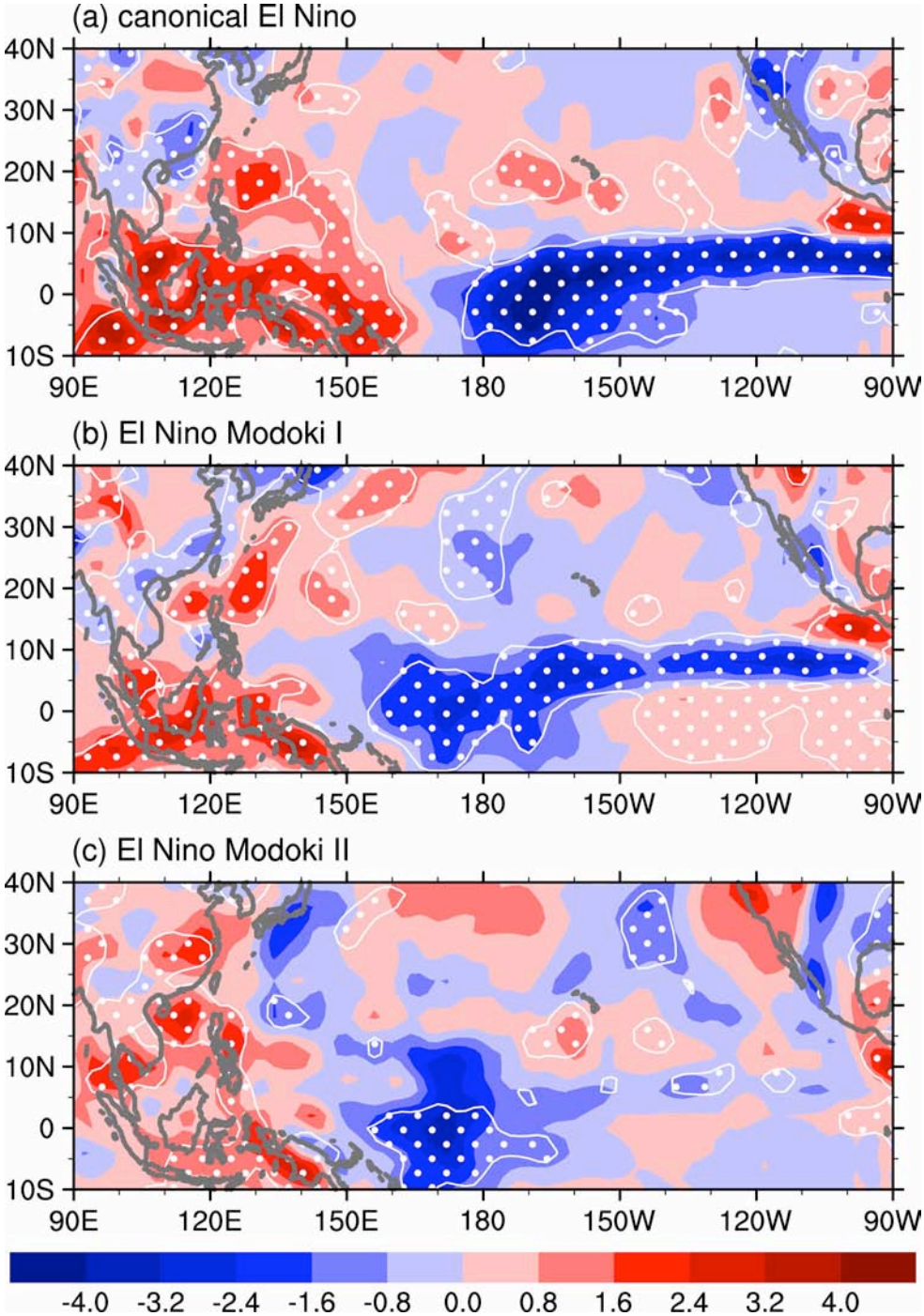


**Figure 7.** Composites of 500-hPa pressure vertical velocity anomalies ($10^{-2}$ Pascal/s) for various El Niño events during fall of the El Niño developing year. Shown are for (a) canonical El Niño, (b) El Niño Modoki I and (c) El Niño Modoki II. The white contours filled with the dots indicate the composite exceeding the 90% significant level, based on Student's *t* test.

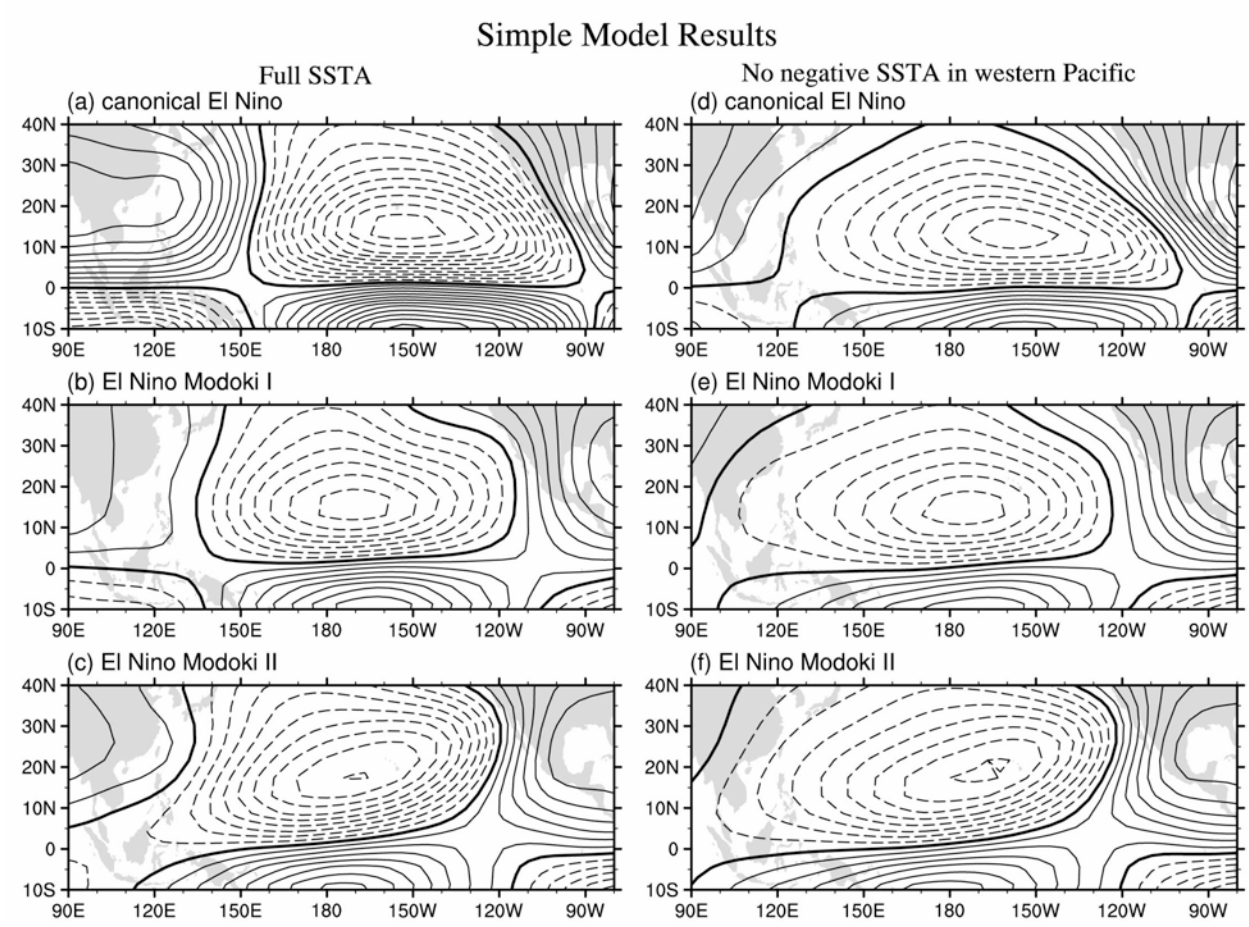


**Figure 8.** Baroclinic streamfunctions ($10^6$ $m^2/s$) from the simple model runs. The left panels show the model response to the SST anomalies (in the region of 110°E-80°W, 30°S-30°N) during fall for canonical canonical El Niño, El Niño Modoki I and El Niño Modoki II in Fig. 4. The right panels show the model response by removing the forcings of negative SST anomalies in the western Pacific. The negative (positive) streamfunction is in dashed (solid) contour. The contour interval is $2.0\times10^6$ $m^2/s$.

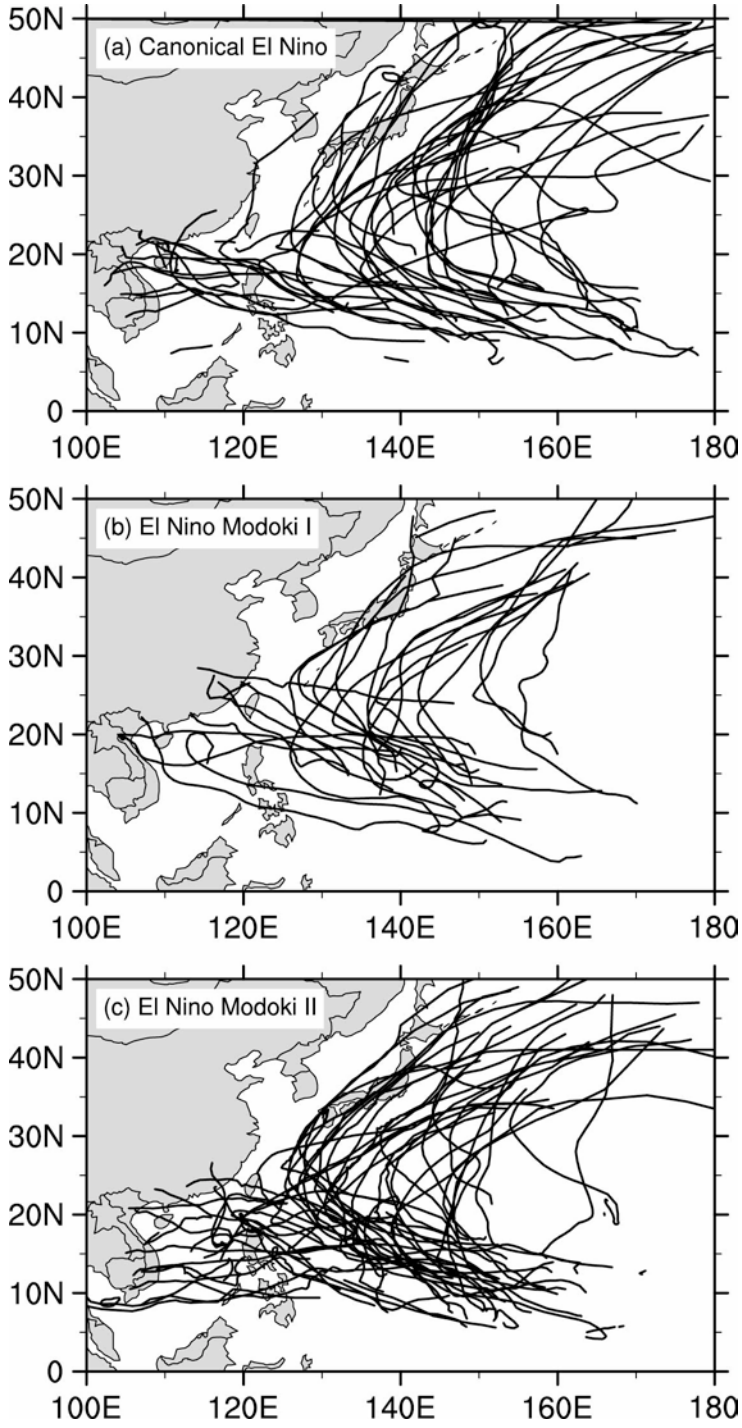


**Figure 9.** The typhoon tracks in the western North Pacific for various El Niño events during fall of the El Niño developing year. Shown are (a) six years of canonical El Niño (1951/52, 1965/66, 1972/73/ 1976/77, 1982/83, and 1997/98), (b) four years of El Niño Modoki I (1963/64, 1987/88, 1990/91, and 2002/03), and (c) six years of El Niño Modoki II (1968/69, 1979/80, 1991/92, 1992/93, 2004/05, and 2009/10).

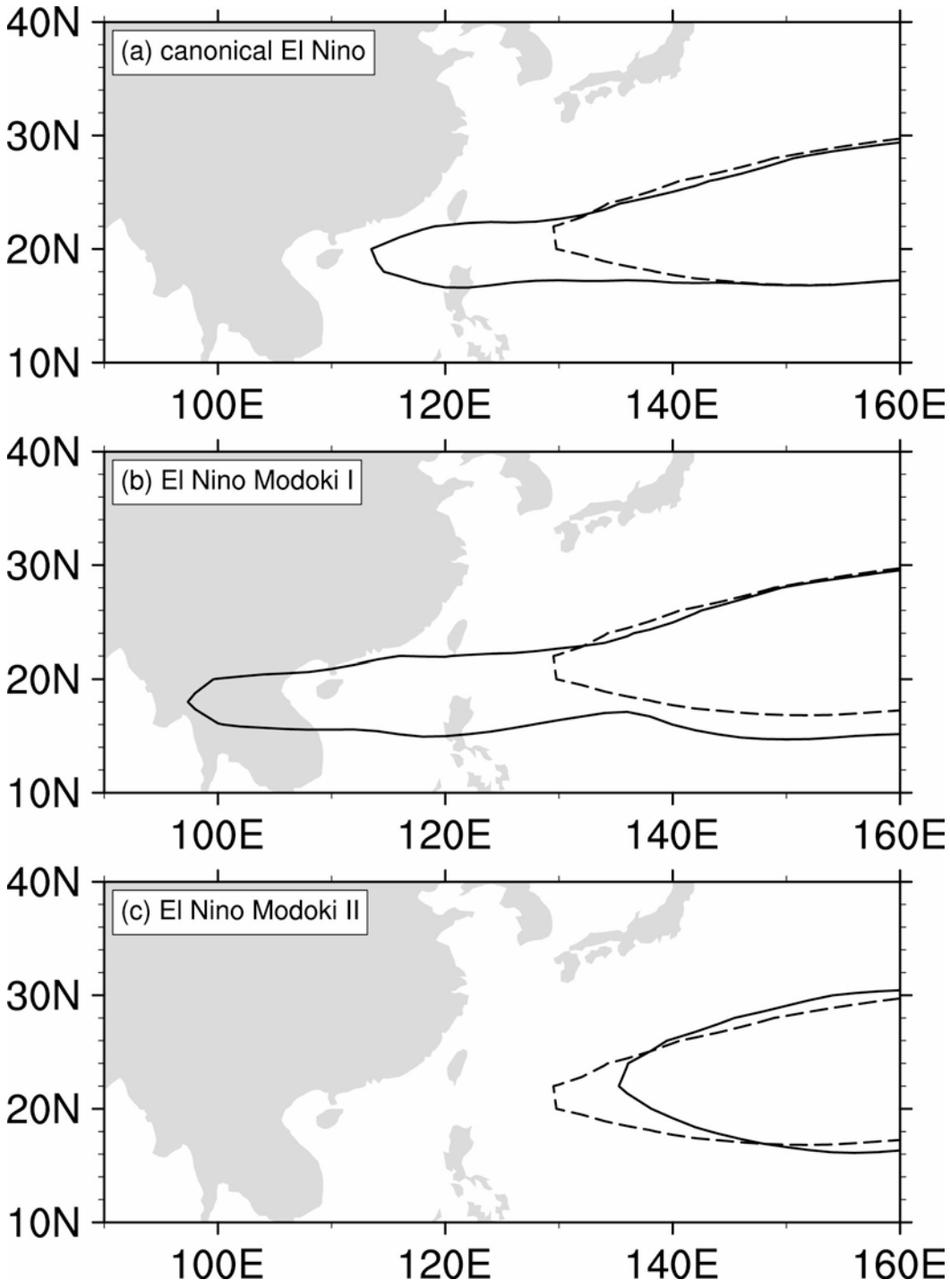


**Figure 10.** Composites of the western North Pacific subtropical high (WNPSH) for various El Niño events during fall of the El Niño developing year. Shown are for (a) canonical El Niño, (b) El Niño Modoki I and (c) El Niño Modoki II. The WNPSH is represented by the contour of 5864 gpm of the 500 hPa geopotential height. The dashed contour line represents the climatological WNPSH.

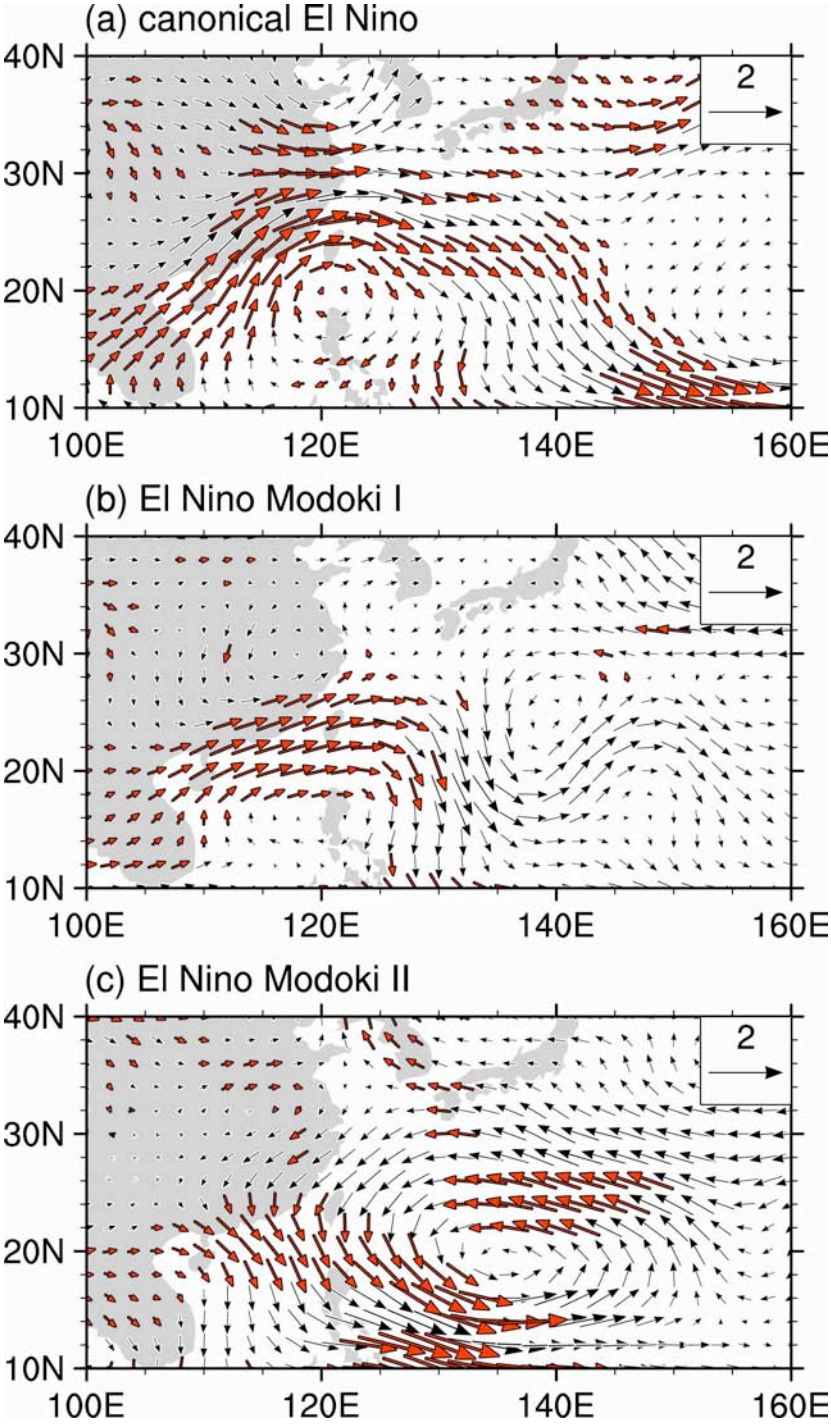


**Figure 11.** Composites of the TC steering flow anomalies ($10^3$ hPa m/s) for various El Niño events during fall of the El Niño developing year. Shown are for (a) canonical El Niño, (b) El Niño Modoki I and (c) El Niño Modoki II. The TC steering flow anomalies are computed by the vertically-averaged wind anomalies in the low troposphere from 950-hPa to 700-hPa. The red vectors indicate the wind amplitude exceeding the 90% significant level, based on Student's *t* test.